



Contents lists available at ScienceDirect

European Journal of Medicinal Chemistry

journal homepage: <http://www.elsevier.com/locate/ejmech>

Research paper

SP1-independent inhibition of FOXM1 by modified thiazolidinediones

Seyed Amirhossein Tabatabaei Dakhili ^a, David J. Pérez ^{a,b}, Keshav Gopal ^a,
Moinul Haque ^{c,d}, John R. Ussher ^a, Khosrow Kashfi ^{e,f}, Carlos A. Velázquez-Martínez ^{a,*}^a Faculty of Pharmacy and Pharmaceutical Sciences, University of Alberta, Edmonton, AB, Canada^b Unidad Radiofarmacia-Ciclotrón, División de Investigación, Facultad de Medicina, Universidad Nacional Autónoma de México, México City, Mexico^c Department of Laboratory Medicine and Pathology, University of Alberta, Edmonton, AB, Canada^d Department of Oncology, University of Alberta, Edmonton, AB, Canada^e Department of Molecular, Cellular, & Biomedical Sciences, City University of New York School of Medicine, New York, USA^f Department of Molecular, Cellular and Biomedical Sciences, Sophie Davis School of Biomedical Education, City University of New York School of Medicine, New York, USA

ARTICLE INFO

Article history:

Received 16 June 2020

Received in revised form

16 September 2020

Accepted 28 September 2020

Available online xxx

Keywords:

FOXM1

Transcription factors

Troglitazone

Thiazolidinediones.

Anticancer

MDA-MB-231

Breast cancer

ABSTRACT

This research article describes an approach to modify the thiazolidinedione scaffold to produce test drugs capable of binding to, and inhibit, the *in vitro* transcriptional activity of the oncogenic protein FOXM1. This approach allowed us to obtain FOXM1 inhibitors that bind directly to the FOXM1-DNA binding domain without targeting the expression levels of Sp1, an upstream transcription factor protein known to activate the expression of FOXM1. Briefly, we modified the chemical structure of the thiazolidinedione scaffold present in anti-diabetic medications such as pioglitazone, rosiglitazone and the former anti-diabetic drug troglitazone, because these drugs have been reported to exert inhibition of FOXM1 but hit other targets as well. After the chemical synthesis of 11 derivatives possessing a modified thiazolidinedione moiety, we screened all test compounds using *in vitro* protocols to measure their ability to (a) dissociate a FOXM1-DNA complex (EMSA assay); (b) decrease the expression of FOXM1 in triple negative-breast cancer cells (WB assay); (c) downregulate the expression of FOXM1 downstream targets (luciferase reporter assays and qPCR); and inhibit the formation of colonies of MDA-MB-231 cancer cells (colony formation assay). We also identified a potential binding mode associated with these compounds in which compound TFI-10, one of the most active molecules, exerts binding interactions with Arg289, Trp308, and His287. Unlike the parent drug, troglitazone, compound TFI-10 does not target the *in vitro* expression of Sp1, suggesting that it is possible to design FOXM1 inhibitors with a better selectivity profile.

© 2020 Elsevier Masson SAS. All rights reserved.

1. Introduction

The Forkhead box M1 protein is a member of a large family of transcription factors that share a unique wing helix DNA binding domain [1], and it is one of the proteins responsible for maintaining normal cell replication by promoting cell cycle progression [2]. In normal cells, FOXM1 is expressed during the S phase; it induces the G1 phase; and it regulates normal cell cycle by expressing a number of G2/M-related genes including PIK1, CCNB2, and Nek2 [3]. From an activation standpoint the FOXM1 protein undergoes multiple phosphorylation reactions exerted by different kinases throughout

the cell cycle, and it becomes transcriptionally active at the G2/M phase [4]. However, it has been observed that differentiated cells have marginal expression levels of FOXM1 [5].

In contrast to its role in normal cell proliferation FOXM1 is overexpressed in cancer cells and it is an essential driving force in tumorigenesis. FOXM1 causes genomic instability and unregulated cell division in a wide variety of human cell carcinomas including lung, oropharyngeal, melanoma, leukemia, pancreatic, and breast tissue [6–12]. The overexpression of this transcription factor is also linked to poor prognosis and resistance to chemotherapeutic agents, which makes FOXM1 both a useful biomarker and a promising drug target [13,14].

We previously proposed a “lead hopping” hypothesis describing how three structurally different FOXM1 inhibitors bind to, and disrupt, the interaction between the FOXM1 protein and its DNA

* Corresponding author.

E-mail address: velazque@ualberta.ca (C.A. Velázquez-Martínez).

binding site [15]. The three drugs involved in our prior publication are the forkhead domain inhibitor-6 (FDI-6), thioestrepton (TSP), and troglitazone (TGZ) (Fig. 1). In addition, we described a drug-binding site at the interface of the FOXM1 protein and its DNA binding domain, through (at least) two binding interactions: (1) a π -sulfur interaction between the aromatic imidazole ring present in His287 and an electron-deficient sulfur atom present in the FOXM1 inhibitors; and (2) a halogen bonding interaction between the 4-fluorophenyl ring in the FDI-6 and Arg297 in the protein. Based on these two previously reported binding interactions, we herein describe the design and biological screening of 11 thiazolidinedione forkhead domain inhibitors (TFI-1 to TFI-11), similar to the former antidiabetic drug TGZ. Even though thiazolidinediones in general, and TGZ in particular, exert their antidiabetic activity by targeting a different transcription factor (the peroxisome proliferator-activated receptor gamma, [PPAR γ]), these drug molecules possess a heterocyclic electron-deficient sulfur atom required to exert binding interactions with the His287 residue in FOXM1, and consequently, this feature makes the thiazolidinedione a useful and promising scaffold to transition from an established PPAR γ -dependent antidiabetic effect, to a FOXM1-dependent anticancer activity.

2. Drug design

The anti-diabetic mechanism of action exerted by thiazolidinediones does not appear to be directly correlated to their inhibitory effect on FOXM1. However, Petrovic et al. report an interesting study in which they propose an *indirect* mechanism of action by which thiazolidinediones significantly decrease the expression of FOXM1 [16], and consists on the inhibition of SP1, one of the upstream proteins that activates the expression of FOXM1 [17]. This report is highly relevant to our investigation because, it proposes indirect FOXM1 inhibition. Nevertheless, we propose that the thiazolidinedione ring also binds to the FOXM1-DNA binding domain, and structural modification of this moiety might produce new molecules with relative selectivity toward FOXM1. More importantly, we hypothesize that it may be possible to bypass the Sp1-dependent FOXM1 inhibition while maintaining a relatively

good potency compared to the parent drugs.

To validate this hypothesis, we designed a series of molecules possessing (a) the thiazolidinedione moiety; (b) a simpler chemical scaffold based on TGZ; (c) eliminate the free rotation around the methylene group ($-\text{CH}_2-$) attached to the thiazolidinedione by using an alkene ($-\text{CH}=\text{}$) instead. This replacement would, in theory, decrease the likelihood of the test drugs to bind to the PPAR γ protein [18]. Consequently, we used a computer-based molecular modeling (docking) protocol to examine a wide variety of functional groups attached to a much simpler benzyloxybenzene ring (Scheme 1). The best scores in the modeling protocol were observed when (1) the R₁ position contained a nitro group ($-\text{NO}_2$), trifluoromethyl ($-\text{CF}_3$), or methyloxycarbonyl ($-\text{CO}_2\text{CH}_3$) ester; (2) the R₂ position contained a methoxy ($-\text{OCH}_3$) or a nitro group. Additionally, to increase the robustness of the structure-activity relationship study, we explored the effect produced by varying the position of the thiazolidinedione ring relative to the methoxy and nitro groups on the benzene ring. The overall drug design strategy is explained schematically in Fig. 2.

3. Results and discussion

3.1. Chemistry

Based on the modeling results described above, we synthesized eleven compounds shown in Scheme 1 (TFI-1 to TFI-11) using the Knoevenagel condensation reaction. We adapted several methods described in the literature to prepare the intermediate compounds TFI-1_(int) to TFI-11_(int) by using microwave assisted synthesis [19–22]. Briefly, a 4-substituted benzylbromide was reacted with the corresponding hydroxybenzaldehyde (2a–2c; 1 eq.) in ethanol, under microwave-assisted heating. After ~12 h, we obtained a series of product intermediates labeled TFI-1_(int) to TFI-11_(int), in excellent yields (80%). Then, based on reported protocols [19] we reacted the thiazolidinedione (3 eq.) with piperidine in ethanol, heating under microwave irradiation at 90 °C for 3 h, to obtain the target products (TFI-1 to TFI-11). All final compounds were the corresponding *Z* isomers, based on the chemical shift, a previously reported methine proton chemical shift [23].

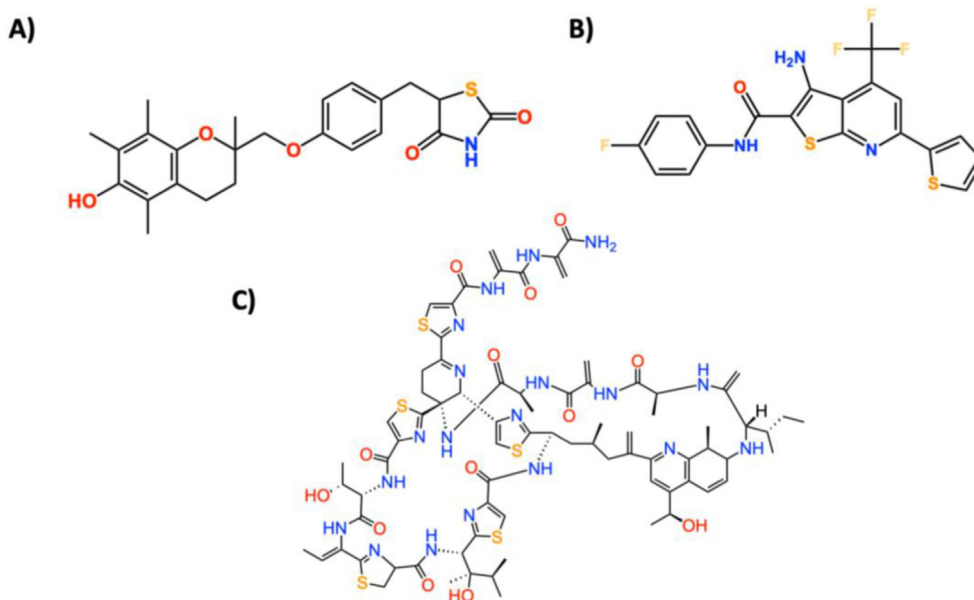
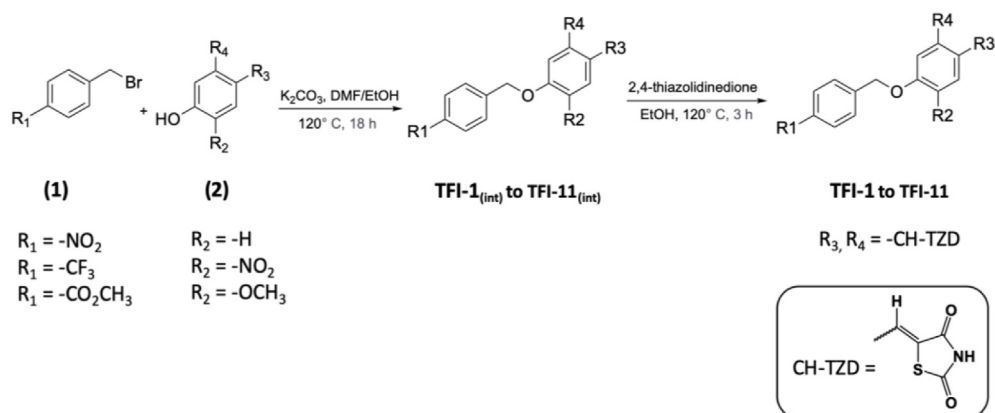


Fig. 1. Current FOXM1 inhibitors. Troglitazone (A) and thioestrepton (B) are known to inhibit FOXM1 indirectly while FDI-6 (C) is the only known selective inhibitor of FOXM1.



Scheme 1. Synthesis and final chemical structures of eleven thiazolidinedione forkhead domain inhibitors TFI-1 to TFI-11.

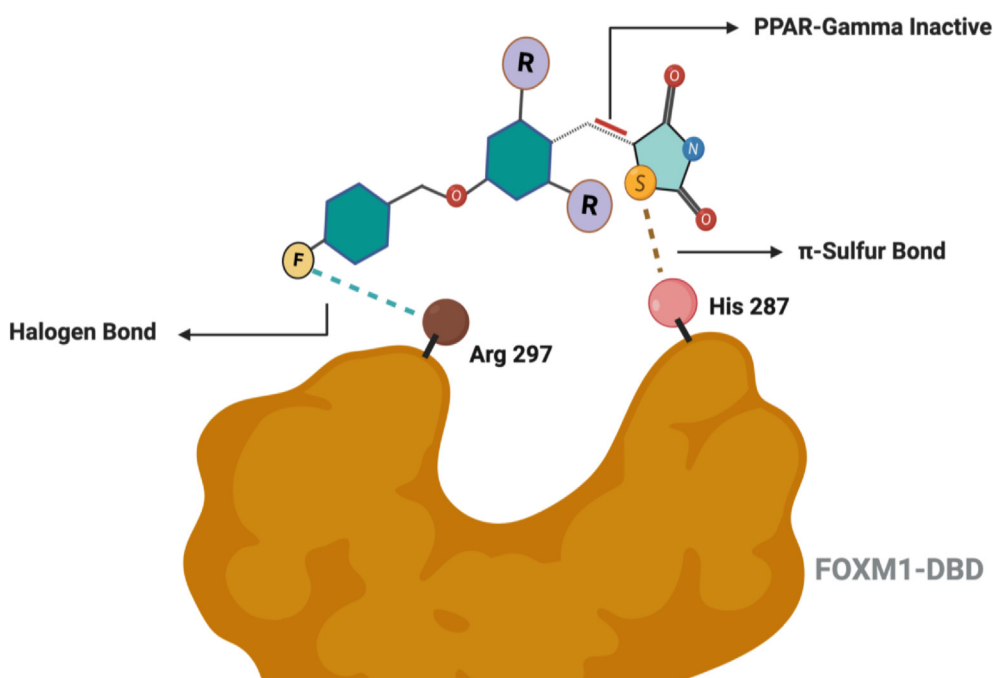


Fig. 2. The drug design strategy for making selective FOXM1 inhibitors. Besides incorporating the π -sulfur interaction of the thiazolidinedione group, we also included halogen bonding between Arg297 and fluorine atom based on our previous finding. Furthermore, the presence of unsaturation has been shown to make the compound PPAR-Gamma non-agonist.

3.2. Western blot assay

To evaluate the potency of the test compounds, first we measured the concentration-dependent effect produced by drug molecules on the protein expression of FOXM1 using a triple negative-breast cancer (TNBC) cell line (MDA-MB-231 cells) after a 48-h incubation period. Fig. 3A shows the results obtained in the Western blot screening assay; we compared the potency of the test compounds (TFI-1 to TFI-11) to that observed with three reference molecules: (a) the parent TGZ, (b) the reported forkhead domain inhibitor FDI-6, and (c) the antibiotic TSP. We observed that compounds TFI-2, TFI-6, and TFI-10 significantly reduced (by more than 90%) protein expression of FOXM1 in MDA-MB-231 cells, while the other derivatives showed a modest activity compared to the reference compounds (80–98% inhibition).

As we were expecting and described in the drug design strategy, most of the compounds having $-CF_3$ group at the R1 position

showed significant activity except for the TFI-7 where the thiazolidinedione was placed at R4 position (too far from His287). According to our modelling study, if the thiazolidinedione is at R4 position, it can't make the π -sulfur interaction with the His287 anymore. Of surprise, compounds carrying nitro groups at the position R1 were also active except for the TFI-4 where an additional nitro group was also introduced in the R2 position. Addition of methoxy group significantly improved the activity of TFI-6 in compare to the TFI-1 where the change was not so expressive when the same functional group was added to the R2 position of TFI-2. All derivatives carrying methyl ester at R1 were inactive irrespective of substitutions at the other sites.

3.3. EMSA and luciferase assay

It is well known in the literature that some FOXM1 inhibitors exert their mechanism of action by either indirect inhibition of

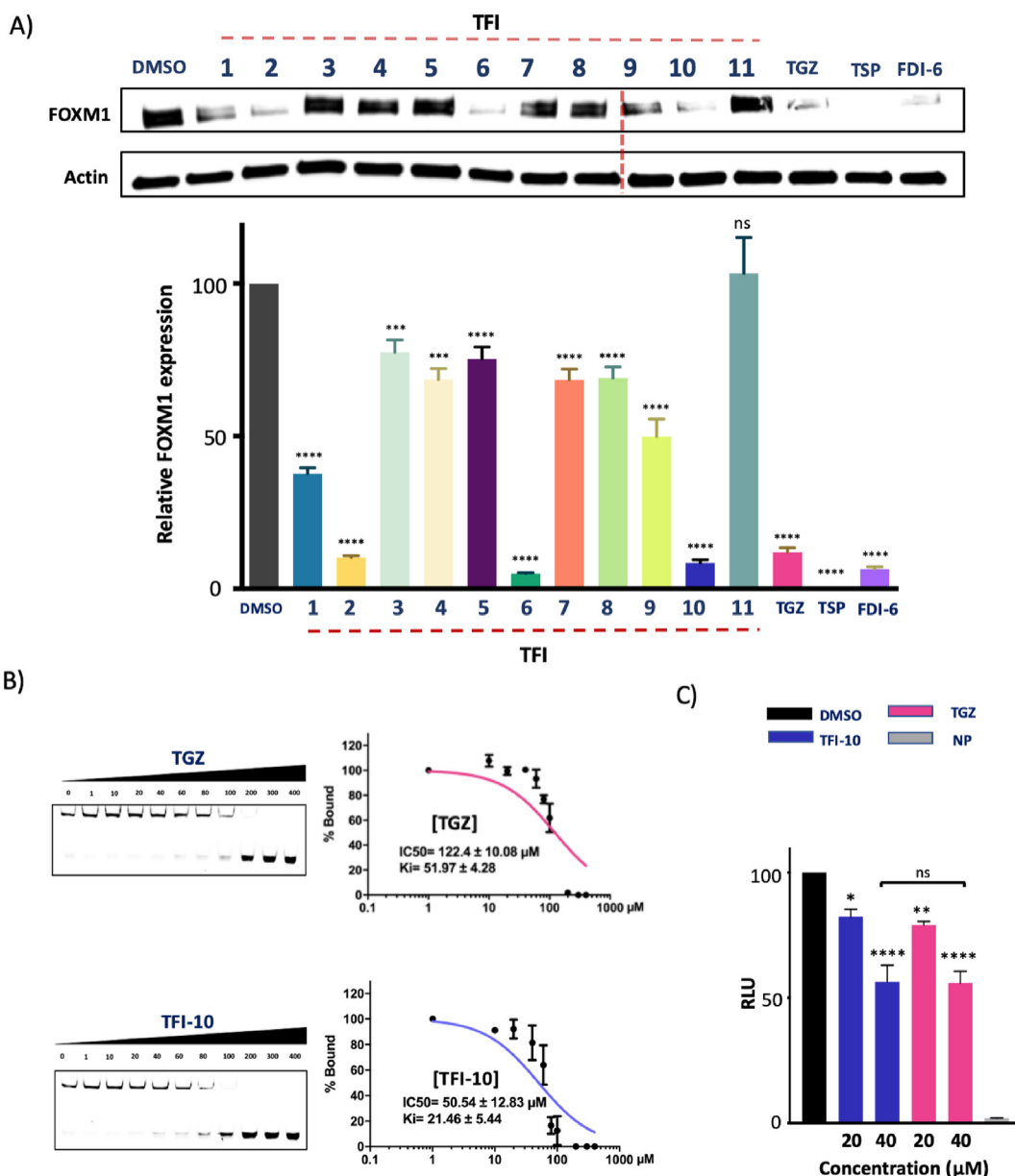


Fig. 3. A) Western blot analysis of FOXM1 protein levels decreased by the test compounds (40 μM; 48 h, MDA-MB-231 cell line). B) electromobility shift assay (EMSA) showing the Ki value determined for the compound TFI-10 and the positive control TGZ; TFI-10 was almost twice as potent as TGZ in preventing the formation of the FOXM1-DNA complex. C) Luciferase reporter assay of the FOXM1 luciferase reporter (the corresponding plasmid was transfected into 293-T cells and the relative level of luciferase activity was measured after incubation of MDA-MB-231 cells with 40 μM of TFI-10 and TGZ, for 24 h). The average values in all experiments were calculated after three independent experiments (n = 3); P values were calculated by one way ANOVA (ns = not significant = P > 0.05; * = P ≤ 0.05; ** = P ≤ 0.01; *** = P ≤ 0.001; **** = P ≤ 0.0001).

upstream FOXM1 activator proteins [24,25] or by increasing the concentration of a negative regulator of the FOXM1 protein, which in turn, is degraded by the proteasome [26,27]. Consequently, to study the mechanism of action exerted by the TGZ derivatives we selected compound TFI-10 to carry out complementary screening assays, and determine if this molecule exerts dissociation of the FOXM1-DNA binding domain using the cell-free electrophoretic mobility shift assay (EMSA; Fig. 3B). The incubation of recombinant FOXM1-DBD and its consensus DNA with the corresponding drug molecules showed that both TGZ and TFI-10 disrupt the complex formed by FOXM1 and DNA. Quantitatively speaking, as shown in Fig. 3B, TGZ and TFI-10 inhibited the protein-DNA complex with a $K_i = 51.9$ nM and 21.4 nM, respectively. This data suggests that compound TFI-10 is about twice as potent than TGZ (Fig. 3B),

suggesting a better inhibitory profile on FOXM1's transcriptional activity.

To evaluate this hypothesis, we incubated MDA-MB-231 cells in the presence of increasing concentrations of test compounds, to determine an IC₅₀ values, using a firefly luciferase reporter assay possessing the corresponding FOXM1 DNA binding sites. In this regard, the relative decrease in FOXM1 transcriptional activity in the presence of the test molecules (Fig. 3C) reproduced the pattern that we previously observed with immunoblotting (Fig. 3A). Both compounds (TFI-10 and TGZ) showed significant activity at both at 20 and 40 μM.

To confirm the results obtained in both the Western blot and the luciferase assays described above, in the sense that any decrease in the expression of the FOXM1 protein would correlate with higher

inhibition of triple negative-breast cancer cell proliferation, we measured the mRNA levels of FOXM1 its downstream target proteins CDC25B and CCNB1. The expression of CCNB1 promotes cell cycle progression (from G2 to M phase) and the expression of CDC25 plays an important role in the cell's M phase [28]. Consistent with our previous protein immunoblot and EMSA experiments, TFI-10 decreased the mRNA levels of the FOXM1 target genes to a higher extent than that produced by TGZ (Fig. 4A).

In a previous report by Petrovic et al. [16] in which it described a thiazolidinedione-induced decrease in the expression of FOXM1, authors reported that this effect is mediated by the inhibition of the transcription factor SP1. Furthermore, Petrovic et al. proposed a new mechanism of action for thiazolidinediones in which this drug class increases the proteasome-dependent degradation of the transcription factor Sp1. Since this protein has a binding domain in the FOXM1 promoter, the activation of Sp1 was associated with an increase in the expression of FOXM1 in cancer cells. Nevertheless, as we showed in Fig. 4B, we observed a significant decrease in the expression levels of SP1 exerted by the parent molecule TGZ, but this effect was not observed when we incubated MDA-MB-231 cells with compound TFI-10, suggesting that TFI-10 inhibits the expression of FOXM1 by a different (SP1-independent) mechanism of action.

Thiazolidinediones (TZDs) are very well studied ligands of the peroxisome proliferator activated receptor gamma (PPAR γ), but this activity, according to Petrovic et al., is not involved in the induction of FOXM1 [16].

Finally, it has been reported that TZDs exert a significant anti-proliferative effect in many epithelial-derived cancer cells by G₁ phase cell cycle arrest through accumulation of the CDK inhibitor proteins p21^{Cip} and p21^{Kip} [29,30], but the investigation of these targets goes beyond the scope of this paper and remains to be explored. Another limitation of our investigation is the observation that other PPAR γ -independent targets of thiazolidinediones are the c-Jun N-terminal protein kinase and p38 [31], the early growth response-1 (EGR1) [32], and the tumor suppressor protein p53 [33]. At this point we do not know if these proteins are targeted by our drug molecule TFI-10 and this will be the subject of upcoming investigations by our group.

3.4. Cell colony formation assay

The sensitization of human carcinoma cells with a FOXM1 inhibitor to conventional chemotherapy (i.e. doxorubicin), via activation of apoptosis, has been studied and reported previously by Halasi et al. [34]. Consequently, we decided to explore if our

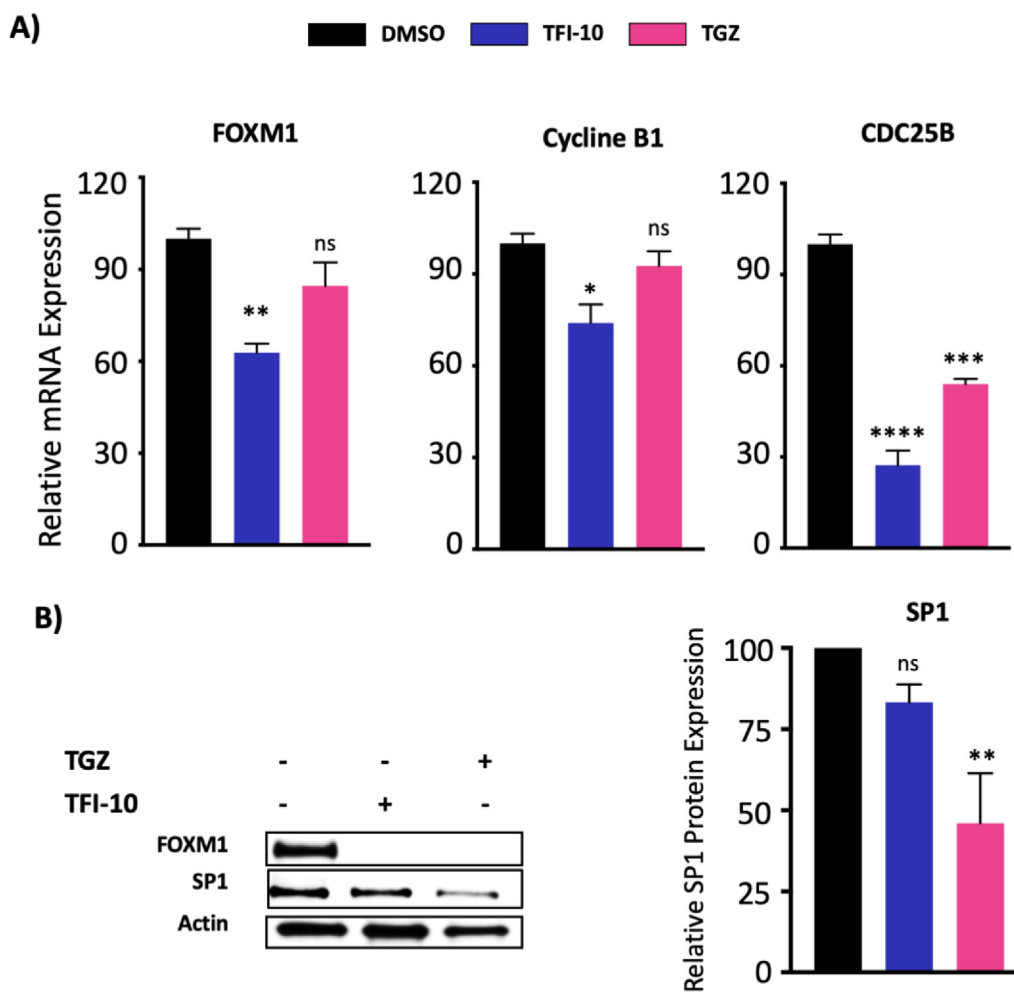


Fig. 4. A) qPCR analysis of mRNA levels of human FOXM1 and its downstream targets including CDC25B and CCNB1. The drug TFI-10 (20 μ M) significantly decreased the mRNA level of FOXM1 target genes at after 24 h, but this effect was not observed with TGZ at the same concentration. B) Western blot assay measuring the expression of the transcription factors SP1 and FOXM1; TGZ and TFI-10 (80 μ M) significantly decreased the level of FOXM1 after 24 h, but the level of SP1 was only affected by TGZ. No significance (ns) = P > 0.05; (*) = P < 0.05; (**) = P < 0.01; (***) = P < 0.001; (****) = P < 0.0001.

thiazolidinedione derivative, TFI-10, is capable of sensitizing human carcinoma cells to DNA-damaging agents. Briefly, cells were initially treated with (a) 5 μM of TFI-10; (b) 50 nM of doxorubicin; or (c) TFI-10 and doxorubicin. As shown in Fig. 5, in contrast to cells treated either with TFI-10 or doxorubicin alone, cells incubated in the presence of both drugs did not form any (detectable) colonies. The results of this experiment agree with those reported by Halasi et al. the inhibition of FOXM1 synergized with the doxorubicin-induced DNA damage in cancer cells. We could speculate that this synergistic effect could be due, at least in part, to inhibition of FOXM1-induced expression of anti-apoptotic factors, such as JNK and Bcl-2 [34].

3.5. Docking and molecular dynamic simulation studies

Finally, to provide a fine-tuned justification for the observed biological profile shown by compound TFI-10, we conducted a computer-based molecular modeling and dynamic simulation study based on a previously reported protocol described by our group in which we proposed a drug-binding pocket at the interface of the FOXM1-DBD. As shown in Fig. 6A, we observed a π -sulfur binding interaction between the thiazolidinedione ring present in TFI-10 and the His287 residue, which agrees with our previous report [15]. The same binding interaction was also observed between His287 and thiazolidinedione ring of the TGZ (Fig. 6B). In this regard, the introduction of a methoxy group to TFI-10 contributed to its increased binding affinity by exerting two hydrogen bonding interactions with Arg286. Furthermore, we also observed an additional binding interaction involving the trifluoromethyl moiety and Trp308, Ser306 and Arg297, providing additional evidence in support of a potential drug binding site at that location. The role of a halogen bonding is not only relevant and significant for the thiazolidinediones reported in this paper, but also for structurally different FOXM1 inhibitors such as the drug FDI-6 reported by Gormally et al. [35].

We also carried out another MD simulation (20 ns) to evaluate the stability of the test compounds inside the proposed binding pocket. It was not surprising for us to see how TFI-10 showed an improved stability inside the binding pocket between FOXM1 and DNA, as quantified by the ligand positional Root Mean Square Deviation (RMSD) (Fig. 6C). Besides that, upon binding, the RMSD values (Fig. 6D) were also decreased, suggesting a higher binding affinity by TFI-10. The side chain Root Mean Square Fluctuation (RMSF) was also utilized to analyze which residues are interacting with the test compounds as shown in Fig. 6E. Finally, the MMPBSA binding free energy was also calculated during the last 5 ns of the drug/FOXM1-DBD simulations. The binding interactions produced

by TFI-10 were better than those observed for TZD, with binding free energies of -103.3 KJ/mol and -82.2 KJ/mol TGZ, respectively (Table 1).

4. Discussion and conclusions

In summary, this research article describes a new approach to modify the thiazolidinedione scaffold to produce derivatives that retain a desirable FOXM1 inhibitory profile, **via an SP1-independent mechanism**, paving the way for the design of novel drug molecules with a good chance of exerting anticancer effects on triple negative-breast cancer cells. We submit evidence demonstrating the direct inhibition of the FOXM1-DNA complex (*in vitro*), and to some extent, transcriptional inhibition of the FOXM1 protein that results in the inhibition of downstream target proteins, as well as significant decrease in cancer cell colony formation (*in vitro*). In this report, we provide preliminary evidence showing that it might be possible to modulate (and bypass) the SP1-dependent anti-cancer mechanism of action exerted by thiazolidinediones, producing relatively potent FOXM1 inhibitors that bind to the target site via (a) π -sulfur interaction, (b) hydrogen bonding, and (c) halogen bonding, reported by our group previously. An additional binding interaction (π - π stacking) observed with the test drug TFI-10 is new to this type of scaffold and it adds to the list of binding interactions for novel FOXM1 inhibitors.

One additional and very important contribution of this research work is the fact that, despite showing a better selectivity profile, compound TFI-10, as well as a wide variety of “direct” FOXM1 inhibitors (including the drugs FDI-6 [35] and TSP [27,36], show weak inhibitory profiles as seen with their *in vitro* IC₅₀ values, regardless of the biological assay employed, the best of them in the low (20–40 μM) range. To our knowledge, there has not been any reports on FOXM1 inhibitors with a significant and potentially useful and “clinically” relevant potency with IC₅₀ values in the low nM range. Therefore, it is reasonable to question whether targeting the FOXM1 protein, at its DNA binding domain, or via inhibition of the proteasome, or inhibiting any of its reported upstream positive modulators, are promising strategies. It is difficult to predict if direct inhibition of the FOXM1 protein will yield drugs potent enough to be considered promising in therapy. Perhaps one of the areas in which direct inhibition of FOXM1 could find a clinical application is combination therapy. As shown in this report, and several others, inhibiting the transcriptional activity of FOXM1 together with chemotherapeutic drugs which depend on a different mechanism of action, seems to be a better strategy that may produce better outcomes, in terms of inhibiting cancer cell proliferation.

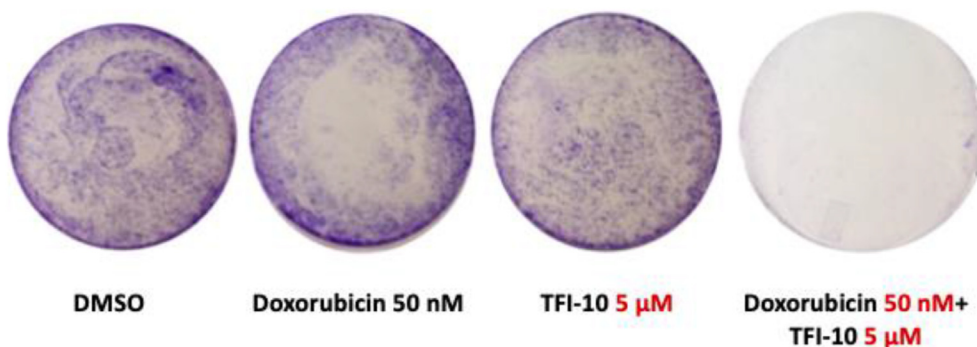


Fig. 5. Colony formation assay using triple negative-breast cancer cells in the presence of test drugs TFI-10, doxorubicin, and a combination of both. Photographs represent the results obtained in one of the three experiments carried out ($n = 3$).

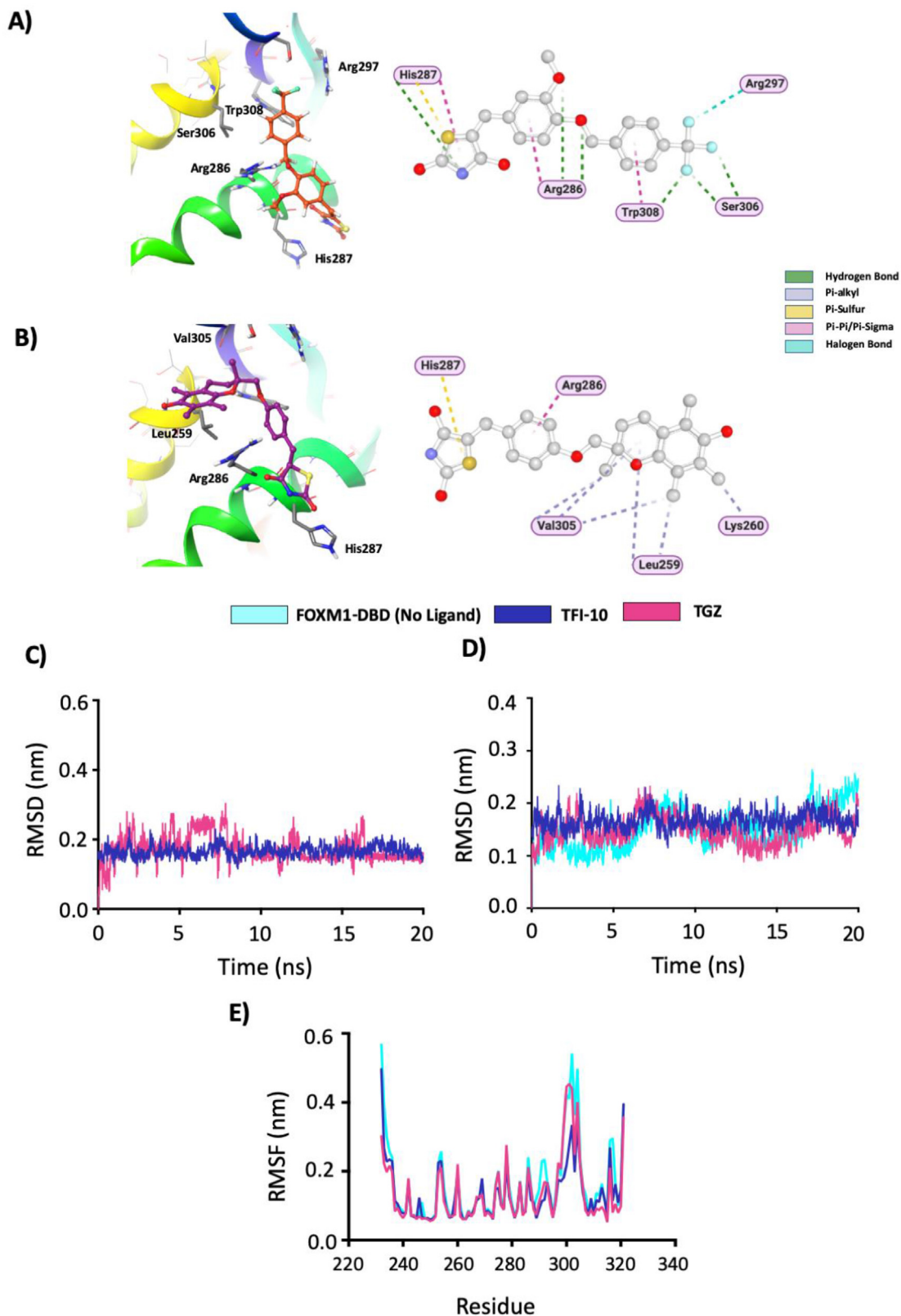


Fig. 6. A) Schematic representation of the drug TFI-10 bound to the FOXM1-DBD showing the expected binding interactions based on a previously reported model; B) Graphical representation of TGZ in complex with the FOXM1-DBD. In addition to the π -sulfur interaction with His287, we observed π -alkyl interactions with Val305, Leu259 and Lys260; C) the calculated ligand positional RMSD for TFI-10 and TGZ suggests higher stability of TFI-10 in the binding pocket; D) RMSD of FOXM1-DBD (no ligand), TFI-10, and TGZ suggesting a strong binding exerted by TFI-10; E) the calculated RMSF values for the FOXM1-DBD (no ligand), TFI-10, and TGZ suggesting a more prominent binding profile of TFI-10, compared to TGZ.

Table 1

MMPBSA binding free energy calculation for TFI-10 and TGZ during the last 5 ns of the simulation. The binding free energy was calculated by subtracting the polar solvation energy from solvent accessible surface area, electrostatic, and VdW energies.

| Compd. | vdW energy | Electrostatic energy | Polar solvation energy | SASA energy | Binding free energy |
|--------|---------------|----------------------|------------------------|-------------|---------------------|
| TFI-10 | -130.8 ± 7.4 | -24.7 ± 5.8 | 65.6 ± 5.9 | -13.4 ± 0.7 | -103.3 ± 6.4 |
| TGZ | -127.6 ± 29.6 | -10.3 ± 5.0 | 70.0 ± 20.6 | -14.2 ± 3.4 | -82.2 ± 17.8 |

5. Experimental

5.1. Chemistry

All the reagents and solvents were purchased from Sigma-Aldrich and were used without further purification. All reactions were monitored by thin-layer chromatography (RediSep® TLC plates) and visualized using UV light. Melting points were measured with an Electrothermal melting point apparatus (ThermoFisher, USA) and were uncorrected. ¹H, ¹³C and ¹⁹F NMR spectra were determined on a Bruker FT-600 MHz instrument (600 MHz, 150 MHz and 565 MHz, respectively) using DMSO-*d*₆ or MeOD as solvents and TMS as a reference. Chemical shifts (δ) and coupling constants (*J*) are expressed in parts per million and Hertz, respectively. Signal multiplicity is expressed as s (singlet), d (doublet), t (triplet), q (quartet), m (multiplet) and br (broad singlet). The microwave-assisted synthesis was carried out using an Initiator Reactor (Biotage).

5.1.1. General procedure for the synthesis of intermediates [TFI-1_(int) to TFI-11_(int)]

We adapted methods described in the literature to prepare the intermediate compounds TFI-1_(int) to TFI-11_(int) by using microwave assisted synthesis [19–22]. The corresponding benzylbromide (1a-1c; 1 eq.), the hydroxybenzaldehyde (2a-2c; 1 eq.), and K₂CO₃ (1 eq.) were mixed in EtOH (5 mL) inside a microwave reactor vessel and heated to 90 °C for 12 h with magnetic stirring. The reactions were monitored by TLC and, upon completion, the final products precipitated as white solid crystals (insoluble in EtOH), which were then filtered off and washed with hot water (5 mL), followed by a second washing with hexane (3 mL); after drying the product intermediates we calculated their purity (about 95%) by ¹H and ¹³C NMR. The overall yields for these reactions was about 80%. Intermediates TFI-1_(int), TFI-3_(int) [19,20,22], and TFI-10_(int) [21], were confirmed by ¹H and ¹³C NMR which were in accordance to the reported analytical data [23].

5.1.1.1. 3-nitro-4-[(4-nitrophenyl)methoxy]benzaldehyde [TFI-4_(int)]. 4-Hydroxy-3-nitrobenzaldehyde (100 mg, 0.598 mmol), 4-nitrobenzyl bromide (129 mg, 0.598 mmol) and K₂CO₃ (83 mg, 0.598 mmol), white crystals, yield 80%. ¹H NMR (600 MHz, DMSO) δ 9.96 (s, 1H), 8.49 (d, *J* = 2.1 Hz, 1H), 8.31 (d, *J* = 8.8 Hz, 2H), 8.22 (dd, *J* = 8.7, 2.1 Hz, 1H), 7.74 (d, *J* = 8.9 Hz, 2H), 7.66 (d, *J* = 8.7 Hz, 1H), 5.62 (s, 2H). ¹³C NMR (151 MHz, DMSO) δ 190.49, 154.85, 147.30, 143.14, 139.56, 135.05, 133.33, 130.58, 129.25, 128.15, 126.74, 124.37, 123.87, 123.81, 116.03, 69.90.

5.1.1.2. Methyl 4-[(4-formyl-2-nitrophenoxy)methyl]benzoate [TFI-5_(int)]. 4-Hydroxy-3-nitrobenzaldehyde (100 mg, 0.598 mmol), methyl 4-(bromomethyl) benzoate (137 mg, 0.598 mmol), K₂CO₃ (83 mg, 0.598 mmol), white crystals, yield 80%. ¹H NMR (600 MHz, DMSO) δ 9.95 (s, 1H), 8.47 (d, *J* = 2.0 Hz, 1H), 8.20 (dd, *J* = 8.7, 2.1 Hz, 1H), 8.01 (d, *J* = 8.3 Hz, 2H), 7.63 (dd, *J* = 20.2, 8.6 Hz, 3H), 5.54 (s, 2H), 3.86 (s, 3H). ¹³C NMR (151 MHz, DMSO) δ 190.47, 165.93, 154.99, 140.83, 139.59, 134.97, 129.47, 129.40, 129.12, 127.37, 126.67, 116.03, 70.42, 52.21.

5.1.1.3. 4-methoxy-3-[(4-nitrophenyl)methoxy]benzaldehyde [TFI-6_(int)]. 3-Hydroxy-4-methoxybenzaldehyde (100 mg, 0.66 mmol), 4-nitrobenzyl bromide (143 mg, 0.66 mmol) and K₂CO₃ (90 mg, 0.66 mmol), white crystals, 80% yield. ¹H NMR (600 MHz, DMSO) δ 9.83 (s, 1H), 8.28 (d, *J* = 8.7 Hz, 2H), 7.73 (d, *J* = 8.8 Hz, 2H), 7.61 (dd, *J* = 8.2, 1.9 Hz, 1H), 7.48 (d, *J* = 1.9 Hz, 1H), 7.24 (d, *J* = 8.3 Hz, 1H), 5.35 (s, 2H), 3.91 (s, 3H). ¹³C NMR (151 MHz, DMSO) δ 191.30, 154.51, 147.76, 147.08, 144.65, 129.58, 128.27, 126.89, 123.66, 111.73, 111.18, 68.69, 56.09.

5.1.1.4. 4-methoxy-3-[(4-(trifluoromethyl)phenyl)methoxy]benzaldehyde [TFI-7_(int)]. 3-Hydroxy-4-methoxybenzaldehyde (100 mg, 0.66 mmol), 4-(trifluoromethyl)benzyl bromide (158 mg, 0.66 mmol), K₂CO₃ (90 mg, 0.66 mmol), white crystals, 90%. ¹H NMR (600 MHz, DMSO) δ 9.83 (s, 1H), 7.78 (d, *J* = 8.0 Hz, 2H), 7.69 (d, *J* = 8.0 Hz, 2H), 7.60 (dd, *J* = 8.2, 1.9 Hz, 1H), 7.49 (d, *J* = 1.9 Hz, 1H), 7.22 (d, *J* = 8.3 Hz, 1H), 5.29 (s, 2H), 3.90 (s, 3H). ¹³C NMR (151 MHz, DMSO) δ 191.31, 154.51, 147.90, 141.61, 129.59, 128.74, 128.53, 128.32, 127.90, 126.94, 126.75, 125.39, 125.36, 125.14, 123.34, 121.54, 111.66, 111.60, 111.09, 68.96, 56.04. ¹⁹F NMR (565 MHz, DMSO) δ -60.96.

5.1.1.5. Methyl 4-[(5-formyl-2-methoxyphenoxy)methyl]benzoate [TFI-8_(int)]. 3-Hydroxy-4-methoxybenzaldehyde (100 mg, 0.66 mmol), methyl 4-(bromomethyl) benzoate (152 mg, 0.66 mmol), K₂CO₃ (90 mg, 0.66 mmol), white crystal, 80%. (TFI-8_(int)). ¹H NMR (600 MHz, DMSO) δ 9.82 (s, 1H), 7.99 (d, *J* = 8.4 Hz, 2H), 7.63–7.56 (m, 3H), 7.47 (d, *J* = 1.9 Hz, 1H), 7.22 (d, *J* = 8.3 Hz, 1H), 5.28 (s, 2H), 3.90 (s, 3H), 3.86 (s, 3H). ¹³C NMR (151 MHz, DMSO) δ 191.31, 166.01, 154.52, 147.93, 142.26, 129.57, 129.36, 129.32, 129.08, 127.59, 127.57, 126.71, 111.66, 111.16, 69.20, 60.76, 56.05, 52.17, 39.52. ¹³C NMR (151 MHz, DMSO) δ 191.31, 166.01, 154.52, 147.93, 142.26, 129.57, 129.36, 129.32, 129.08, 127.59, 127.57, 126.71, 111.66, 111.16, 69.20, 60.76, 56.05, 52.17.

5.1.1.6. 3-Methoxy-4-[(4-nitrophenyl)methoxy]benzaldehyde [TFI-9_(int)]. 4-Hydroxy-3-methoxybenzaldehyde (100 mg, 0.65 mmol), 4-nitrobenzyl bromide (142 mg, 0.65 mmol), K₂CO₃ (90 mg, 0.65 mmol), white crystals, 80%. ¹H NMR (600 MHz, DMSO) δ 9.85 (s, 1H), 8.28 (d, *J* = 8.8 Hz, 2H), 7.73 (d, *J* = 8.8 Hz, 2H), 7.55 (dd, *J* = 8.2, 1.9 Hz, 1H), 7.45 (d, *J* = 1.8 Hz, 1H), 7.25 (d, *J* = 8.3 Hz, 1H), 5.40 (s, 2H), 3.87 (s, 3H). ¹³C NMR (151 MHz, DMSO) δ 191.43, 152.64, 149.44, 147.15, 144.25, 130.17, 128.39, 125.75, 123.70, 112.84, 109.94, 68.76, 55.69.

5.1.1.7. Methyl 4-[(4-formyl-2-methoxyphenyl)methoxy]benzoate [TFI-11_(int)]. 4-Hydroxy-3-methoxybenzaldehyde (100 mg, 0.65 mmol), methyl 4-(bromomethyl) benzoate (150 mg, 0.65 mmol), K₂CO₃ (90 mg, 0.65 mmol). ¹H NMR (600 MHz, DMSO) δ 9.84 (s, 1H), 7.99 (d, *J* = 8.2 Hz, 2H), 7.60 (d, *J* = 8.1 Hz, 2H), 7.54 (dd, *J* = 8.2, 1.9 Hz, 1H), 7.43 (d, *J* = 1.8 Hz, 1H), 7.24 (d, *J* = 8.3 Hz, 1H), 5.32 (s, 2H), 3.85 (s, 6H). ¹³C NMR (151 MHz, DMSO) δ 191.43, 166.00, 152.89, 149.44, 141.89, 130.04, 129.41, 129.21, 127.73, 127.71, 125.81, 112.78, 109.87, 69.32, 55.66, 52.19.

5.1.2. General procedure for the synthesis of compounds TFI-1 - TFI-11

We adapted the methods previously reported [19] to use a microwave-assisted synthesis protocol. The corresponding intermediate (TFI-1_(int) to TFI-11_(int), 1eq.), thiazolidinedione (3 eq.), piperidine (cat.), AcOH (cat.), and EtOH (5 mL), were mixed in a microwave reactor vessel and heated at 90 °C for 3 h, under magnetic stirring. Once completed, the reactions were allowed to cool down to RT to yield a pale yellowish precipitate that was filtered off and washed with cold EtOH (10 mL) and water (10 mL). The target products were obtained with an overall yield of about 60%. In this regard, compound TFI-2 [19], was confirmed by ¹H and ¹³C NMR which was in accordance with the reported data. All derivatives were determined to be the corresponding Z isomers according to a previously reported methine proton chemical shift [23].

5.1.2.1. (5Z)-5-({4-[(4-nitrophenyl)methoxy]phenyl}methylidene)-1,3-thiazolidine-2,4-dione (TFI-1). Thiazolidinedione (67 mg, 0.57 mmol), TFI-1_(int) (50 mg, 0.19 mmol), piperidine (cat.) and AcOH (cat.), pale yellowish crystals, 60% yield, m.p. 251–253 °C ¹H NMR (600 MHz, DMSO) δ 12.52 (br, 1H), 8.27 (d, J = 8.8 Hz, 2H), 7.78–7.69 (m, 3H), 7.58 (d, J = 8.8 Hz, 2H), 7.20 (d, J = 8.9 Hz, 2H), 5.37 (s, 2H). ¹³C NMR (151 MHz, DMSO) δ 168.02, 167.56, 159.58, 147.12, 144.45, 132.12, 131.60, 128.37, 126.11, 123.69, 120.84, 115.76, 68.27. [M – H]⁻: m/z calc. 355.0 found 355.1 m/z (100%).

5.1.2.2. (5Z)-5-[(4-[(trifluoromethyl)phenyl]methoxy}phenyl)methylidene]-1,3-thiazolidine-2,4-dione (TFI-2).

Thiazolidinedione (63 mg, 0.54 mmol), TFI-2_(int) (50 mg, 0.18 mmol), piperidine (cat.) and AcOH (cat.), pale yellowish crystals, 60% yield, m.p. 202–203 °C. ¹H NMR (600 MHz, DMSO) δ 12.53 (br, 1H), 7.77 (d, J = 8.2 Hz, 2H), 7.75 (s, 1H), 7.68 (d, J = 8.1 Hz, 2H), 7.58 (d, J = 8.8 Hz, 2H), 7.19 (d, J = 8.8 Hz, 2H), 5.32 (s, 2H). ¹³C NMR (151 MHz, DMSO) δ 167.97, 167.49, 159.72, 141.44, 132.11, 131.65, 128.56, 128.35, 128.13, 125.97, 125.43, 125.40, 120.69, 115.74, 68.54, 56.02. ¹⁹F NMR (565 MHz, DMSO) δ –60.96. [M – H]⁻: m/z calc. 378.0 found 378.2 m/z (100%).

5.1.2.3. Methyl 4-({4-[(Z)-(2,4-dioxo-1,3-thiazolidin-5-ylidene)methyl]phenyl}methoxy)benzoate (TFI-3).

Thiazolidinedione (64 mg, 0.55 mmol), TFI-3_(int) (50 mg, 18.5 mmol), piperidine (cat.) and AcOH (cat.). (TFI-3), pale yellowish crystals, 60% yield, m.p. 220–222 °C. ¹H NMR (600 MHz, DMSO) δ 12.53 (br, 1H), 7.99 (d, J = 8.4 Hz, 2H), 7.74 (s, 1H), 7.59 (dd, J = 20.4, 8.6 Hz, 4H), 7.18 (d, J = 8.9 Hz, 2H), 5.30 (s, 2H), 3.86 (s, 3H). ¹³C NMR (151 MHz, DMSO) δ 167.97, 167.49, 165.98, 165.47, 159.79, 142.07, 141.99, 132.09, 131.67, 129.39, 129.35, 129.13, 127.62, 127.61, 125.92, 120.64, 115.74, 68.78, 60.77, 52.18. [M – H]⁻: m/z calc. 368.1 found 368.1 m/z (100%).

5.1.2.4. (5Z)-5-({3-nitro-4-[(4-nitrophenyl)methoxy]phenyl}methylidene)-1,3-thiazolidine-2,4-dione (TFI-4).

Thiazolidinedione (59.73 mg, 0.51 mmol), TFI-4_(int) (50 mg, 0.17 mmol), piperidine (cat.) and AcOH (cat.), pale yellowish crystals, 60% yield, m.p. 242–243 °C. ¹H NMR (600 MHz, DMSO) δ 12.68 (br, 1H), 8.30 (d, J = 8.8 Hz, 1H), 8.21 (d, J = 2.2 Hz, 1H), 7.88 (dd, J = 9.1, 2.3 Hz, 1H), 7.81 (s, 1H), 7.74 (d, J = 8.9 Hz, 1H), 7.60 (d, J = 9.0 Hz, 1H), 5.57 (s, 1H). ¹³C NMR (151 MHz, DMSO) δ 167.63, 151.55, 147.27, 143.36, 139.63, 135.23, 129.15, 128.12, 126.89, 126.28, 123.80, 116.39, 69.65. [M – H]⁻: m/z calc. 400.0 found 400.3 m/z (100%).

5.1.2.5. Methyl 4-({4-[(Z)-(2,4-dioxo-1,3-thiazolidin-5-ylidene)methyl]-2-nitrophenoxy}methyl)benzoate (TFI-5).

Thiazolidinedione (56.2 mg, 0.51 mmol), TFI-5_(int) (50 mg, 0.16 mmol), piperidine (cat.) and AcOH (cat.), pale yellowish crystals, 60% yield, m.p. 225–227 °C. ¹H NMR (600 MHz, DMSO) δ 12.67

(br, 1H), 8.19 (d, J = 2.2 Hz, 1H), 8.00 (d, J = 8.4 Hz, 2H), 7.85 (dd, J = 9.1, 2.3 Hz, 1H), 7.81 (s, 1H), 7.59 (t, J = 8.5 Hz, 3H), 5.49 (s, 2H), 3.86 (s, 3H). ¹³C NMR (151 MHz, DMSO) δ 167.49, 167.22, 165.94, 151.74, 141.03, 139.64, 135.18, 129.46, 129.35, 127.33, 126.87, 126.04, 123.93, 116.39, 70.17, 52.21. [M – H]⁻: m/z calc. 413.0 found 413.2 m/z (100%).

5.1.2.6. (5Z)-5-({4-methoxy-3-[(4-nitrophenyl)methoxy]phenyl}methylidene)-1,3-thiazolidine-2,4-dione (TFI-6).

Thiazolidinedione (61 mg, 0.52 mmol), TFI-6_(int) (50 mg, 0.17 mmol), piperidine (cat.) and AcOH (cat.), pale yellowish crystals, 60% yield, m.p. 200–202 °C. ¹H NMR (600 MHz, DMSO) δ 12.50 (br, 1H), 8.27 (d, J = 8.8 Hz, 1H), 7.73 (d, J = 8.8 Hz, 1H), 7.69 (s, 1H), 7.24–7.19 (m, 1H), 7.18 (d, J = 9.0 Hz, 1H), 5.33 (s, 1H), 3.87 (s, 2H). ¹³C NMR (151 MHz, DMSO) δ 167.95, 167.37, 151.15, 147.39, 147.08, 144.70, 131.89, 128.28, 125.60, 124.56, 123.67, 120.73, 115.10, 112.56, 68.78, 55.88. [M – H]⁻: m/z calc. 385.1 found 385.3 m/z (100%).

5.1.2.7. (5Z)-5-[(4-methoxy-3-[(4-(trifluoromethyl)phenyl]methoxy}phenyl)methylidene]-1,3-thiazolidine-2,4-dione (TFI-7).

Thiazolidinedione (56.2 mg, 0.48 mmol), TFI-7_(int) (50 mg, 0.16 mmol), piperidine (cat.) and AcOH (cat.), pale yellow crystals, 60% yield, m.p. 203–205 °C. ¹H NMR (600 MHz, DMSO) δ 12.50 (br, 1H), 7.77 (d, J = 8.2 Hz, 2H), 7.70 (s, 1H), 7.68 (d, J = 8.1 Hz, 2H), 7.24–7.19 (m, 2H), 7.16 (d, J = 8.3 Hz, 2H), 5.27 (s, 2H), 3.86 (s, 3H). ¹³C NMR (151 MHz, DMSO) δ 167.95, 167.39, 151.15, 147.53, 141.63, 131.94, 128.76, 128.55, 128.34, 128.13, 128.06, 126.94, 125.60, 125.42, 125.40, 125.37, 125.35, 125.14, 124.47, 123.33, 121.53, 120.68, 114.99, 112.50, 69.04, 55.83. ¹⁹F NMR (565 MHz, DMSO) δ –60.96. [M – H]⁻: m/z calc. 408.1 found 408.3 m/z (100%).

5.1.2.8. Methyl 4-({5-[(Z)-(2,4-dioxo-1,3-thiazolidin-5-ylidene)methyl]-2-methoxyphenyl}methoxy)benzoate (TFI-8).

Thiazolidinedione (53 mg, 0.45 mmol), TFI-8_(int) (50 mg, 0.15 mmol), piperidine (cat.) and AcOH (cat.), pale yellowish crystals, 60% yield, m.p. 233–236 °C. ¹H NMR (600 MHz, DMSO). ¹H NMR (600 MHz, DMSO) δ 12.50 (br, 1H), 7.99 (d, J = 8.4 Hz, 2H), 7.69 (s, 1H), 7.60 (d, J = 8.5 Hz, 2H), 7.21 (dd, J = 4.3, 2.4 Hz, 2H), 7.17 (d, J = 9.0 Hz, 1H), 5.26 (s, 2H), 3.86 (s, J = 3H), 3.85 (s, 3H). ¹³C NMR (151 MHz, DMSO) δ 167.98, 167.41, 166.01, 165.50, 151.17, 147.58, 142.30, 142.22, 131.93, 129.38, 129.36, 129.34, 129.08, 127.59, 127.57, 127.55, 125.58, 124.49, 120.67, 115.00, 112.50, 69.28, 60.76, 55.84, 52.16. [M – H]⁻: m/z calc. 398.1 found 398.2 m/z (100%).

5.1.2.9. (5Z)-5-({3-methoxy-4-[(4-nitrophenyl)methoxy]phenyl}methylidene)-1,3-thiazolidine-2,4-dione (TFI-9).

Thiazolidinedione (60 mg, 0.52 mmol), TFI-9_(int) (50 mg, 0.17 mmol), piperidine (cat.) and AcOH (cat.), pale yellowish crystals, 65% yield, m.p. 205–208 °C. ¹H NMR (600 MHz, DMSO) δ 12.53 (br, 1H), 8.27 (d, J = 8.8 Hz, 2H), 7.75 (s, 1H), 7.72 (d, J = 8.9 Hz, 2H), 7.25 (d, J = 2.0 Hz, 1H), 7.17 (dt, J = 8.4, 5.1 Hz, 2H), 5.42 (s, 2H), 3.85 (s, 3H). ¹³C NMR (151 MHz, DMSO) δ 167.97, 149.26, 149.22, 147.11, 144.52, 131.96, 128.35, 126.45, 123.69, 123.39, 113.78, 113.71, 68.68, 55.72. [M – H]⁻: m/z calc. 385.1 found 385.1 m/z (100%).

5.1.2.10. (5Z)-5-[(3-methoxy-4-[(4-(trifluoromethyl)phenoxy]methyl]phenyl)methylidene]-1,3-thiazolidine-2,4-dione (TFI-10).

Thiazolidinedione (56 mg, 0.48 mmol), TFI-10_(int) (50 mg, 0.16 mmol), piperidine (cat.) and AcOH (cat.), pale yellowish crystals, 65% yield, m.p. 201–203 °C. ¹H NMR (600 MHz, DMSO) δ 12.51 (br, 1H), 7.78 (d, J = 8.0 Hz, 2H), 7.74 (s, 1H), 7.67 (d, J = 8.1 Hz, 2H), 7.24 (s, 1H), 7.18 (dd, J = 22.6, 8.5 Hz, 2H), 5.30 (s, 2H), 3.84 (s, 3H). ¹³C NMR (151 MHz, DMSO) δ 167.97, 167.43, 149.39, 149.24, 141.49, 132.03, 128.77, 128.56, 128.35, 128.15, 126.93, 126.30, 125.45, 125.43, 125.40, 125.38, 125.13, 123.46, 123.32, 120.89, 113.67, 68.95, 55.68.

^{19}F NMR (565 MHz, DMSO) δ -60.95. [M - H] $^-$: m/z calc. 408.1 found 408.3 m/z (100%).

5.1.2.11. Methyl4-((4-[(Z)-(2,4-dioxo-1,3-thiazolidin-5-ylidene)methyl]-2-methoxyphenoxy)methyl)benzoate (TFI-11). Thiazolidinedione (56 mg, 0.48 mmol), TFI-11_(int) (50 mg, 0.16 mmol), piperidine (cat.) and AcOH (cat.), yellowish crystals, 60% yield, m.p. 212–214 °C. ^1H NMR (600 MHz, DMSO) δ 12.53 (br, 1H), 7.99 (d, J = 8.4 Hz, 2H), 7.75 (s, 1H), 7.59 (d, J = 8.5 Hz, 2H), 7.24 (d, J = 2.0 Hz, 1H), 7.16 (dt, J = 8.6, 5.3 Hz, 2H), 5.28 (s, 2H), 3.86 (s, 3H), 3.84 (s, 3H). ^{13}C NMR (151 MHz, DMSO) δ 167.97, 167.42, 166.00, 149.47, 149.25, 142.13, 132.04, 129.38, 129.13, 127.71, 127.66, 126.26, 125.80, 123.45, 120.85, 113.70, 113.65, 112.78, 109.86, 69.30, 69.21, 55.68, 55.65, 52.18. [M - H] $^-$: m/z calc. 398.1 found 398.2 m/z (100%).

5.2. Cell culture

The MDA-MB-231 cancer cell line was a gift from Dr. Frank Wuest (Cross Cancer Institute; Edmonton, Alberta, Canada). RPMI media was supplemented with 10% fetal bovine serum (FBS) in a 5% CO₂ atmosphere at 37 °C to grow and maintain the cells.

5.3. Colony formation assay

MDA-MB-231 cells were plated at 3×10^5 Confluence and treated with different concentration of compound **TFI-10**. After 24 h the cells were trypsinized, resuspended and counted. 750 cells were then seeded and incubated for 10 days and media Renewed on the 4th day. On the 10th day, media was removed from the petri dishes and washed once with cold PBS. The colonies were stained with 5 mL of 1% Crystal Violet for 30 min. The dishes were fixed by methanol and rinsed with water three times, air-dried and the colonies were counted using Imagej.

5.4. Western blot

6 well plates (3×10^5 confluency) were treated at different concentrations for 24 h. Then, the cells were washed twice with ice cold PBS before incubating and extracting with RIPA lysis buffer (ThermoFisher) for 30 min. The protein levels were quantified using the Bradford assay prior to loading of 40 μg of protein into a 10% SDS-PAGE (Sodium dodecyl sulfate Polyacrylamide gel electrophoresis). Upon completion of the run, the proteins were transferred from the gel to a nitrocellulose membrane (ThermoFisher) and blocked with 10% fat-free milk in TBST for 45 min. The corresponding antibody was incubated with the membrane (1:1000 dilution) at 4 °C overnight. Next day, the membrane was washed with TBST before incubating the appropriate secondary antibody for 45 min at RT. Then, the membrane was washed three times (15 min total) with TBST and the conjugated protein bands were visualized by adding the Chemiluminescence reagent (ThermoFisher) using ImageQuant™ LAS 4000 mini biomolecular imager (GE Healthcare Life Sciences). The quantification was carried out for all proteins relative to β -Actin using Imagej. We used a FOXM1 monoclonal (mouse, sc-271746) antibody; SP1 monoclonal (mouse, sc-420) antibody; β -Actin monoclonal (mouse, sc-47778) antibodies and anti-mouse (sc-516102) and anti-rabbit (sc-2030) secondary antibodies from Santa Cruz Biotechnology.

5.5. Protein expression and purification

BL21 (DE3) competent cells were used to transform the PEX-N-GST FOXM1-DBD plasmid (OriGene Technologies, USA). Next, positive colonies on LB agar media supplemented with ampicillin

(100 $\mu\text{g}/\text{mL}$) were selected and grown in LB media (100 $\mu\text{g}/\text{mL}$ ampicillin) at 37 °C until they reached the optical density (OD600) of 0.8 and then 1 mM isopropyl β -D-1-thiogalactopyranoside (IPTG) was added. After 6 h incubation at 37 °C, the supernatant layer was purified using glutathione resin (GenScript, USA) following the manufacturer's instructions.

5.6. Electrophoretic mobility shift assay

For the protein-DNA complex dissociation experiments we used recombinant FOXM1-DBD, which was incubated with the corresponding compound for 1.5 h at RT [35]. Then its target DNA oligo (Forward strand: 5'-/IRD700/-AAACAAACAAACAATCAAACAAACAAACAATC-3') was incubated with the mixture for 20 min in a buffer solution composed of 20 mM Tris (pH 7.5), 100 mM KCl, 1 mM EDTA, 0.1 mM DTT, and 10% glycerol. The mixture was then loaded on a non-denaturing 6% polyacrylamide gel for 30 min at 120 V. The K_i value was calculated based on the previously determined K_d (Data not shown) value using the following formula Eq. (1):

$$K_i = \frac{[I]}{\left(\frac{[I]_{50}}{K_d} + \frac{[P]_0}{K_d + 1}\right)} \quad \text{Eq. (1)}$$

where: [I]50 = IC50 of the inhibitor; [L]50 = concentration of IR-labeled DNA at 50% inhibition; [P] = concentration of the FOXM1 protein; and K_d = dissociation constant calculated from the initial titration curve.

5.7. Luciferase reporter assay

The 6x-FOXM1 firefly luciferase reporter and its corresponding backbone plasmid-pGL4.10 (i.e empty reporter) were gifts from Drs. Carter J Barger and Adam R. Karpf. Briefly, MD-MB-231 cells were transiently transfected with equal amounts of the 6x-FOXM1 and empty luciferase reporter plasmids. Following 24 h incubation, cells were treated with 40 μM of drug for 12 h. Cells were then washed with cold PBS and lysed with Reporter Lysis Buffer (Promega). Protein concentration was estimated, and equal amounts of total protein from each lysate was analyzed for firefly luciferase activity using the Luciferase Reporter Assay System (Promega). Assays were performed in triplicates.

5.8. Quantitative real time PCR (qPCR)

The RNeasy Mini Kit (Qiagen, Valencia, CA) was used to isolate total RNA from cell lines. Trace DNA was removed on column through DNA digestion with DNase I (Invitrogen, Carlsbad, CA). 1 μg of total RNA was used to prepare cDNA with the High-Capacity cDNA Reverse Transcription Kit (Invitrogen, Carlsbad, CA). qPCR reactions were prepared in 96-well plates (Invitrogen, Carlsbad, CA) with the PowerUp™ SYBR™ Green Master Mix (Invitrogen, Carlsbad, CA) according to manufacturer's protocol. The Mastercycler® ep Realplex system (Eppendorf, Hamburg, Germany) was used for cycling and detecting amplification. Primers for all genes have been validated in prior studies and were purchased from Invitrogen. Sequences of the primers used in this study include: FOXM1: F-5-CGTCGGCCACTGATTCTCAA-3 & R- 5-GGCAGGGGATCTCTAGGTTC-3, CDC25B: F-5-CCTCCGAATCTTCTGATGCAG-3 & R- 5-GCGTCTGATGGCAAACCTGC-3, CCNB1: F-5-GTAATGTTGTA-GAGTTGGTGCC-3 & R- 5-CATGGTGCACTTCTCCTT-3, GAPDH: F-5/GGTCTCCTCTGACTTCAACACGC-3 & R- 5 ACCACCTGTTGCTGTAGCCAA-3. qPCR cycling was setup as denaturation at 95 °C for 10 min, followed by 40 cycles at 95 °C for 15 s, annealing &

extension at 60 °C for 1 min. The relative gene expression was determined using the $\Delta\Delta$ -CT method. For each treatment group, target gene expression was normalized to *GAPDH* expression followed by normalization of target gene expression to the control treatment.

5.9. Molecular modeling and molecular dynamic simulation

The crystal structure of FOXM1-DBD [37], was retrieved from Protein data bank (PDB_ID: 3G73). Chimera v 1.10.12 [38], was used to prepare the structure followed by the charge assignment of protonated groups to pH 7 using PROPKA. MD simulation of the FOXM1-DBD was performed using Gromacs 2018 package. We solvated the protein complex in a box with TIP3P water model with 1 nm margin on each side. The system was further neutralized with NaCl before performing the steepest descent minimization using the AMBER99SBOILDN force field. The system was gradually heated to 300 K using Berendsen thermostat while the pressure was maintained and equilibrated at 1 bar with Parrinello-Rahman barostat respectively. Finally, while maintaining the periodic boundary condition, 50 ns production run was performed. The Particle Mesh Ewald (PME) summation and Lenard-Jones were used to calculate the long range electrostatic and VDW interaction respectively. Next, TFI-10 and TGZ were docked in the FOXM1-DBD binding pocket (previously reported and validated) using Autodocktools and the AnteChamber Python Parser Interface (ACPYPE) was used to generate their parameters. The binding free energy of the TFI-10 and TGZ was calculated using G_MMPBSA as previously reported. Root Mean Square Deviation (RMSD), Root Mean Square Fluctuation (RMSF) and for the complex, Ligand positional RMSD were calculated using the Gromacs package and the graphs were plotted using Graphpad Prism 8. Schrodinger's Maestro and Discovery Studio Visualizer 32, were used to visualize and make the figures.

Declaration of competing interest

The authors declare that they have no known competing financial interests or personal relationships that could have appeared to influence the work reported in this paper.

Acknowledgements

Authors acknowledge the support from the Noujaim Fund for Strategic Initiatives, Faculty of Pharmacy and Pharmaceutical Sciences, University of Alberta. The National Council for Science and Technology (CONACYT) provided a fellowship for D.J.P (CVU: 287012). This research was enabled in part by Compute Canada and its regional partner WestGrid. The graphical abstract and Fig. 2 were created using the program provided by BioRender.

Appendix A. Supplementary data

Supplementary data to this article can be found online at <https://doi.org/10.1016/j.ejmech.2020.112902o>.

References

- [1] D. Nandi, P.S. Cheema, N. Jaiswal, A. Nag, FoxM1: repurposing an oncogene as a biomarker, *Semin. Canc. Biol.* 52 (2018) 74–84, <https://doi.org/10.1016/j.semcancer.2017.08.009>.
- [2] F.C. Kelleher, H. O'Sullivan, FOXM1 in sarcoma: role in cell cycle, pluripotency genes and stem cell pathways, *Oncotarget* 7 (2016) 42792–42804, <https://doi.org/10.18632/oncotarget.8669>.
- [3] N. Chai, H.H. Xie, J.P. Yin, K.D. Sa, Y. Guo, M. Wang, J. Liu, X.F. Zhang, X. Zhang, H. Yin, Y.Z. Nie, K.C. Wu, A.G. Yang, R. Zhang, FOXM1 promotes proliferation in human hepatocellular carcinoma cells by transcriptional activation of CCNB1,

- Biochem. Biophys. Res. Commun.* 500 (2018) 924–929, <https://doi.org/10.1016/j.bbrc.2018.04.201>.
- [4] M. Halasi, A.L. Gartel, Targeting FOXM1 in cancer, *Biochem. Pharmacol.* 85 (2013) 644–652, <https://doi.org/10.1016/j.bcp.2012.10.013>.
- [5] M. Halasi, B. Pandit, M. Wang, V. Nogueira, N. Hay, A.L. Gartel, Combination of oxidative stress and FOXM1 inhibitors induces apoptosis in cancer cells and inhibits xenograft tumor growth, *Am. J. Pathol.* 183 (2013) 257–265, <https://doi.org/10.1016/j.ajpath.2013.03.012>.
- [6] I.M. Kim, T. Ackerson, S. Ramakrishna, M. Tretiakova, I.C. Wang, T. V. Kalin, M.L. Major, G.A. Gusarova, H.M. Yoder, R.H. Costa, V.V. Kalinichenko, The Forkhead Box m1 transcription factor stimulates the proliferation of tumor cells during development of lung cancer, *Canc. Res.* 66 (2006) 2153–2161, <https://doi.org/10.1158/0008-5472.CAN-05-3003>.
- [7] P.A. Madureira, R. Varshochi, D. Constantinidou, R.E. Francis, R.C. Coombes, K.M. Yao, E.W. Lam, The Forkhead box M1 protein regulates the transcription of the estrogen receptor alpha in breast cancer cells, *J. Biol. Chem.* 281 (2006) 25167–25176, <https://doi.org/10.1074/jbc.M603906200>.
- [8] H. Wang, D.I. Hammoudeh, A. V. Follis, B.E. Reese, J.S. Lazo, S.J. Metallo, E. V. Prochownik, Improved low molecular weight Myc-Max inhibitors, *Mol. Canc. Therapeut.* 6 (2007) 2399–2408, <https://doi.org/10.1158/1535-7163.MCT-07-0005>.
- [9] S. Nakamura, I. Hirano, K. Okinaka, T. Takemura, D. Yokota, T. Ono, K. Shigeno, K. Shibata, S. Fujisawa, K. Ohnishi, The FOXM1 transcriptional factor promotes the proliferation of leukemia cells through modulation of cell cycle progression in acute myeloid leukemia, *Carcinogenesis* 31 (2010) 2012–2021, <https://doi.org/10.1093/carcin/bgq185>.
- [10] K.M. Huynh, J.W. Soh, R. Dash, D. Sarkar, P.B. Fisher, D. Kang, FOXM1 expression mediates growth suppression during terminal differentiation of HO-1 human metastatic melanoma cells, *J. Cell. Physiol.* 226 (2011) 194–204, <https://doi.org/10.1002/jcp.22326>.
- [11] J.R. Janus, R.R. Laborde, A.J. Greenberg, V.W. Wang, W. Wei, A. Trier, S.M. Olsen, E.J. Moore, K.D. Olsen, D.I. Smith, Linking expression of FOXM1, CEP55 and HELLS to tumorigenesis in oropharyngeal squamous cell carcinoma, *Laryngoscope* 121 (2011) 2598–2603, <https://doi.org/10.1002/lary.22379>.
- [12] X. Song, S.S. Fiati Kenston, J. Zhao, D. Yang, Y. Gu, Roles of FoxM1 in cell regulation and breast cancer targeting therapy, *Med. Oncol.* 34 (2017) 41, <https://doi.org/10.1007/s12032-017-0888-3>.
- [13] D.W. Chan, S.Y. Yu, P.M. Chiu, K.M. Yao, V.W. Liu, A.N. Cheung, H.Y. Ngan, Over-expression of FOXM1 transcription factor is associated with cervical cancer progression and pathogenesis, *J. Pathol.* 215 (2008) 245–252, <https://doi.org/10.1002/path.2355>.
- [14] J.T. Xia, H. Wang, L.J. Liang, B.G. Peng, Z.F. Wu, L.Z. Chen, L. Xue, Z. Li, W. Li, Overexpression of FOXM1 is associated with poor prognosis and clinico-pathologic stage of pancreatic ductal adenocarcinoma, *Pancreas* 41 (2012) 629–635, <https://doi.org/10.1097/MPA.0b013e31823bcef2>.
- [15] S.A. Tabatabaei-Dakhili, R. Aguayo-Ortiz, L. Domínguez, C.A. Velázquez-Martínez, Untying the knot of transcription factor druggability: molecular modeling study of FOXM1 inhibitors, *J. Mol. Graph. Model.* 80 (2018) 197–210, <https://doi.org/10.1016/j.jmgm.2018.01.009>.
- [16] V. Petrovic, R.H. Costa, L.F. Lau, P. Raychaudhuri, A.L. Tyner, Negative regulation of the oncogenic transcription factor FoxM1 by thiazolidinediones and mithramycin, *Canc. Biol. Ther.* 9 (2010) 1008–1016, <https://doi.org/10.4161/cbt.9.12.11710>.
- [17] X. Kong, L. Li, Z. Li, X. Le, C. Huang, Z. Jia, J. Cui, S. Huang, L. Wang, K. Xie, Dysregulated expression of FOXM1 isoforms drives progression of pancreatic cancer, *Canc. Res.* 73 (2013) 3987–3996, <https://doi.org/10.1158/0008-5472.CAN-12-3859>.
- [18] J.-W. Huang, C.-W. Shiau, Y.-T. Yang, S.K. Kulp, K.-F. Chen, R.W. Bruggemeier, C.L. Shapiro, C.-S. Chen, Peroxisome proliferator-activated receptor γ -independent ablation of cyclin D1 by thiazolidinediones and their derivatives in breast cancer cells, *Mol. Pharmacol.* 67 (2005) 1342–1348, <https://doi.org/10.1124/mol.104.007732>.
- [19] B.R. Bhattarai, B. Kafle, J.-S. Hwang, D. Khadka, S.-M. Lee, J.-S. Kang, S.W. Ham, I.-O. Han, H. Park, H. Cho, Thiazolidinedione derivatives as PTP1B inhibitors with antihyperglycemic and antiobesity effects, *Bioorg. Med. Chem. Lett.* 19 (2009) 6161–6165, <https://doi.org/10.1016/j.bmcl.2009.09.020>.
- [20] K. Bhooshan, A.N. G. K. Deegendra, P. Hwangseo, C. Hyeongjin, Isoxazol-5(4H) one derivatives as PTP1B inhibitors showing an anti-obesity effect, *Chem. Asian J.* 6 (2011) 2073–2079, <https://doi.org/10.1002/asia.201100154>.
- [21] R. Carrasco-Gomez, S. Keppner-Witter, M. Hieke, L. Lange, G. Schneider, M. Schubert-Zsilavecz, E. Proschak, B. Spänkuch, Vanillin-derived anti-proliferative compounds influence Plk1 activity, *Bioorg. Med. Chem. Lett.* 24 (2014) 5063–5069, <https://doi.org/10.1016/j.bmcl.2014.09.015>.
- [22] M. Hrast, K. Rožman, M. Jukić, D. Patin, S. Gobec, M. Sova, Synthesis and structure-activity relationship study of novel quinazolinone-based inhibitors of Mura, *Bioorg. Med. Chem. Lett.* 27 (2017) 3529–3533, <https://doi.org/10.1016/j.bmcl.2017.05.064>.
- [23] Y. Momose, K. Meguro, H. Ikeda, C. Hatanaka, S. Oi, T. Sohda, Studies on antidiabetic agents. X. Synthesis and biological activities of pioglitazone and related compounds, *Chem. Pharm. Bull.* 39 (1991) 1440–1445, <https://doi.org/10.1248/cpb.39.1440>.
- [24] S. Blagden, J. de Bono, Drugging cell cycle kinases in cancer therapy, *Curr. Drug Targets* 6 (2005) 325–335, <https://doi.org/10.2174/1389450053765824>.
- [25] J. Rader, M.R. Russell, L.S. Hart, M.S. Nakazawa, L.T. Belcastro, D. Martinez, Y. Li,

- E.L. Carpenter, E.F. Attiyeh, S.J. Diskin, S. Kim, S. Parasuraman, G. Caponigro, R.W. Schnepf, A.C. Wood, B. Pawel, K.A. Cole, J.M. Maris, Dual CDK4/CDK6 inhibition induces cell-cycle arrest and senescence in neuroblastoma, *Clin. Canc. Res.* 19 (2013) 6173–6182, <https://doi.org/10.1158/1078-0432.CCR-13-1675>.
- [26] A.L. Gartel, Mechanisms of apoptosis induced by anticancer compounds in melanoma cells, *Curr. Top. Med. Chem.* 12 (2012) 50–52, <https://doi.org/10.2174/156802612798919196>.
- [27] A.L. Gartel, A new target for proteasome inhibitors: FoxM1, *Expert Opin. Invest. Drugs* 19 (2010) 235–242, <https://doi.org/10.1517/13543780903563364>.
- [28] E. Schmitt, R. Boutros, C. Froment, B. Monsarrat, B. Ducommun, C. Dozier, CHK1 phosphorylates CDC25B during the cell cycle in the absence of DNA damage, *J. Cell Sci.* 119 (2006) 4269–4275, <https://doi.org/10.1242/jcs.03200>.
- [29] H. Koga, S. Sakisaka, M. Harada, T. Takagi, S. Hanada, E. Taniguchi, T. Kawaguchi, K. Sasatomi, R. Kimura, O. Hashimoto, T. Ueno, H. Yano, M. Kojiro, M. Sata, Involvement of p21(WAF1/Cip1), p27(Kip1), and p18(INK4c) in troglitazone-induced cell-cycle arrest in human hepatoma cell lines, *Hepatology* 33 (2001) 1087–1097, <https://doi.org/10.1053/jhep.2001.24024>.
- [30] S. Takeuchi, T. Okumura, W. Motomura, M. Nagamine, N. Takahashi, Y. Kohgo, Troglitazone induces G1 arrest by p27(Kip1) induction that is mediated by inhibition of proteasome in human gastric cancer cells, *Japanese J. Cancer Res.* 93 (2002) 774–782, <https://doi.org/10.1111/j.1349-7006.2002.tb01319.x>.
- [31] M.A. Bae, B.J. Song, Critical role of c-Jun N-terminal protein kinase activation in troglitazone-induced apoptosis of human HepG2 hepatoma cells, *Mol. Pharmacol.* 63 (2003) 401–408, <https://doi.org/10.1124/mol.63.2.401>.
- [32] S.J. Baek, L.C. Wilson, L.C. Hsi, T.E. Eling, Troglitazone, a peroxisome proliferator-activated receptor gamma (PPAR gamma) ligand, selectively induces the early growth response-1 gene independently of PPAR gamma. A novel mechanism for its anti-tumorigenic activity, *J. Biol. Chem.* 278 (2003) 5845–5853, <https://doi.org/10.1074/jbc.M208394200>.
- [33] T. Okura, M. Nakamura, Y. Takata, S. Watanabe, Y. Kitami, K. Hiwada, Troglitazone induces apoptosis via the p53 and Gadd45 pathway in vascular smooth muscle cells, *Eur. J. Pharmacol.* 407 (2000) 227–235, [https://doi.org/10.1016/S0014-2999\(00\)00758-5](https://doi.org/10.1016/S0014-2999(00)00758-5).
- [34] M. Halasi, A.L. Gartel, Suppression of FOXM1 sensitizes human cancer cells to cell death induced by DNA-damage, *PLoS One* 7 (2012), e31761, <https://doi.org/10.1371/journal.pone.0031761>.
- [35] M. V Gormally, T.S. Dexheimer, G. Marsico, D.A. Sanders, C. Lowe, D. Matak-Vinkovic, S. Michael, A. Jadhav, G. Rai, D.J. Maloney, A. Simeonov, S. Balasubramanian, Suppression of the FOXM1 transcriptional programme via novel small molecule inhibition, *Nat. Commun.* 5 (2014) 5165, <https://doi.org/10.1038/ncomms6165>.
- [36] A.L. Gartel, FoxM1 inhibitors as potential anticancer drugs, *Expert Opin. Ther. Targets* 12 (2008) 663–665, <https://doi.org/10.1517/14728222.12.6.663>.
- [37] D.R. Littler, M. Alvarez-Fernandez, A. Stein, R.G. Hibbert, T. Heidebrecht, P. Aloy, R.H. Medema, A. Perrakis, Structure of the FoxM1 DNA-recognition domain bound to a promoter sequence, *Nucleic Acids Res.* 38 (2010) 4527–4538, <https://doi.org/10.1093/nar/gkq194>.
- [38] E.F. Pettersen, T.D. Goddard, C.C. Huang, G.S. Couch, D.M. Greenblatt, E.C. Meng, T.E. Ferrin, UCSF Chimera—a visualization system for exploratory research and analysis, *J. Comput. Chem.* 25 (2004) 1605–1612, <https://doi.org/10.1002/jcc.20084>.